Articles
doi.org/10.1002/batt.202100041

Chemistry Europe
European Chemical Societies Publishing

Rechargeable Thin-Film Lithium Microbattery Using a Quasi-Solid-State Polymer Electrolyte

Victor Chaudoy,[a] Fabien Pierre,[b] Arunabh Ghosh,[a, f] Michael Deschamps,[c, d] Francois Tran Van,[a] and Fouad Ghamouss*[a, e]

A thin-film microbattery was designed after synthesizing a unique gel polymer electrolyte (GPE), using polyvinylidene fluoride-co-hexafluoropropylene (PVdF-HFP) and cross-linked poly(ethylene oxide) (PEO), with an ionic liquid and salt (LiTFSI) mixture. The polymers resulted in a semi-interpenetrated polymer network (semi-IPN), hosting an ionic liquid (IL)/salt mixture, and thus exhibited high ionic conductivity and excellent mechanical properties. Nuclear magnetic resonance (NMR) diffusion measurements and relaxation rates analysis highlighted the existence of interactions between Li^+ ions and oxygen within the polymers, preventing electrolyte leakage and ensuring excellent mechanical strength which enabled a unique quasi-solid electrolyte. Such mechanical strength and chemical stability made this electrolyte to be first ever reported GPE to withstand thermal evaporation deposition and hence direct deposition of lithium metal. The electrolyte could be shaped as self-standing thin films, and thus worked as both separator and electrolyte in a thin-film lithium microbattery. The thin-film microbattery exhibited excellent performances showing no short-circuit current, an open circuit voltage of ~3.0 V, higher nominal voltage plateau, lower equivalent series resistance by comparison to a thin-film microbattery designed in conventional way with a popular ceramic electrolyte LiPON.

1. Introduction

In present time, we have witnessed an ever-increasing demand for the electrical micro-storage systems like micro-batteries, because of rapid and vast developments of several smart, miniaturized, and autonomous systems.[1] The emerging IoT enabled smart and comfortable lifestyles, including wearable devices, implantable medical devices, smart homes, other miniaturized flexible electronics, do require flexible micro-batteries, with flexibility limit thickness ($<500\ \mu m$), yet with suitable mechanical strength and stabilities.[2] Therefore, there has always been is a strong urge for the development of microbatteries since the earlier demonstration by Kanehori et al. in 1983.[3] Since then, many electrodes and electrolytes were investigated to improve both electrochemical window and charge storage performances of these microbattery systems.[4] In the early 1990's, Bates et al. reported Li_3PO_4 thin films, deposited by RF sputter deposition in the presence of nitrogen gas resulted in a nitrogen-doped lithium phosphate (LiPON). This material showed no grain-boundary, good electrochemical stability and reduced electronic conductivity.[5–7] LiPON therefore remained as one of the most frequently employed electrolytes for all-solid state micro-batteries. LiPON or other solid-state electrolytes offer noticeable advantages over the liquid counterparts, such as prevention of accidental leakage, ease of packaging and safety. However, in order to realize the complete full cell fabrication of a microbattery, the good mechanical properties and low reactivity of LiPON or other solid-state electrolytes are required.[6] The use of LiPON is limited because of the low ionic conductivity ($10^{-6}\ S\,cm^{-1}$ at 30 °C), which induces a high internal resistance of the microbattery. Moreover, formation of LiPON layers, through processes like RF magnetron sputtering, is a time and energy consuming process. Finally, the biggest challenge with non-polymer solid-state electrolytes is that they suffer from the formations of highly resistive interfacial layers at the electrode/electrolyte interfaces.[8,9] Because of the rigid (non-fluidic) nature of non-polymer solid-state electrolytes, the contact area between the electrode surface and the solid electrolyte is inherently limited. Therefore, a "softer" electrolyte should be ideal for minimizing interfacial resistance at the electrode/electrolyte interface.[10] Replacing LiPON or ceramic based electrolytes by a polymer and/or a GPE is a

[a] Dr. V. Chaudoy, Dr. A. Ghosh, Prof. F. Tran Van, Prof. F. Ghamouss
PCM2E, EA 6299
Université de Tours
Parc de Grandmont, 37200 Tours, France
E-mail: fouad.ghamouss@univ-tours.fr
[b] Dr. F. Pierre
ST Microelectronics SAS
16 rue Pierre et Marie Curie, F-37100 Tours, France
[c] Prof. M. Deschamps
CNRS UPR 3079 CEMHTI
Orléans University
45100 Orléans, France
[d] Prof. M. Deschamps
RS2E, French Network for Electrochemical Energy Storage
FR CNRS 3459
80039 Amiens, France
[e] Prof. F. Ghamouss
Materials Science, Energy and Nano-Engineering (MSN) Department
Mohammed VI Polytechnic University (UM6P)
Hay Moulay Rachid, Lot 660 Benguerir, Morocco
[f] Dr. A. Ghosh
LE STUDIUM Loire Valley Institute for Advanced Studies
1, rue Dupanloup, 45000 Orleans, France

Supporting information for this article is available on the WWW under https://doi.org/10.1002/batt.202100041

promising strategy to solve such internal resistance issues of the electrochemical microdevices, as well as to decrease the cost of the process.[1]

Polymer electrolytes have unique advantages, such as, remarkable safety features, no volatility issues, no or minimum leakage, adaptability to a wide variety of fabrication methods in desirable size and shape, also polymers are of lightweight and adaptable to economic packaging structures.[11,12] In comparison to LiPON, a GPE requires an inexpensive deposition process (spin coating, spray coating, hand coating, inkjet or screen printing), and hence can be easily used for microbattery fabrications in different shapes and sizes, like in-plane microbattery based on the interdigital patterns, 3D microbattery architecture.[13,14] GPEs derived from organic and organometallic molecules appeared as the best choice as a non-corrosive, low toxicity, and biocompatible electrolyte for microbatteries. enabling applications like flexible implantable orthodontic systems, and other flexible IoT applications.[15–17] However, the main challenges in the fabrication of polymer electrolytes are to obtain high enough ionic conductivity while retaining all other good physical properties intact. The first GPE studies were essentially based on the swelling of a polymer membrane in organic solvents with lithium salt.[18] However, the volatility and the flammability of organic solvents limits the compatibility with various applications and vacuum processes.[19] Many polar polymers can dissolve salts and dissociates them, but the fact is, not each of them can guarantee enough ionic conductivity.[20] PVdF and its copolymer PVdF-HFP, polyvinyl chloride (PVC), polyacrylonitrile (PAN), poly(methyl methacrylate) (PMMA), PEO have been extensively studied as polymer matrices either in the form of gels or as solid films.[21–25] In order to develop an effective electrolyte with high ionic conductivity, the polymer should not only be capable of dissolving the salt, but also to be able to couple with the lithium salt to have the ionic motion along with the polymer chains. At this point, PEO and its derivatives appeared as very promising, thanks to their lone pair of oxygens on the PEO segment, which can be coordinated to the lithium ion by Coulombic interactions, causing the anion and cation of the lithium salt to dissociate. Here, PEO acts as a solvent, and the lithium salt gets dissolved into the PEO matrix.[26] However, PEO/Li salt possesses a very low ambient temperature conductivity ($< 10^{-7}$ S cm^{-1}), restricts them from its practical applications. Therefore, several attempts to improve PEO's ionic conductivities were observed. Such as introduction of inorganic fillers, chemical functionalization of its polymeric chains, the copolymerization or design of interpenetrating cross-linked networks etc.[27–33]

In recent years, room-temperature ionic liquids (RTILs) have been intensively investigated to be formulated with PEO, to improve its conductivities and other properties suitable for being used as an electrolyte. RTILs satisfy many requirements of being an ideal plasticizing salts when used with PEO, improving not only ionic conductivities, but also improved the thermal properties, and also expanding the temperatures in quasi solid electrolytes for lithium-based battery systems.[34,35] Moreover, ILs are preferred thanks to their non-volatile nature, non-flammability, non-toxicity, reasonably good conductivity, excellent thermal and/or chemical stability, and higher electrochemical potential windows.[36–38] Associated with PEO, and thanks to their non-volatility they could be favorably used with processes needing low vacuum such as physical deposition. There are reports on ILs/PEO based solid polymer matrices to optimize between ionic conductivity, modify mechanical and transport properties, wider electrochemical window and other physical and mechanical properties.[39–43] Moreover, it was found that free RTILs in a polymer matrix can undergo percolation, resulting in a highly conductive pathway across the electrolyte and creates an interfacial layer with improved wettability, which greatly improves the interfacial compatibility with the electrodes.[44] In addition, the conductivities of GPEs can be easily tuned by changing the relative amount of IL within a polymer matrix. However, high ionic conductivity which usually means high amount of liquid phase within the polymer matrix, should not be achieved at the expense of the electrolyte films' integrity and mechanical stability.[26,45] Generally speaking, GPEs can display poor mechanical strengths compared to their solid-state counterparts. Therefore, it is necessary to design a GPE with reasonably good mechanical strength in thin film, so that it is compatible with processes like lithium deposition through thermal evaporation, which is subject to an ultra-vacuum environment (~10^{-7} mbar).

Therefore, in this work, we designed a self-supporting thin-film GPE, with an optimized composition that is compatible with the lithium metal deposition process by thermal evaporation technique. This industry-friendly efficient technique was used for the making of a full cell microbattery based on GPE. Here we chose PEO along with a porous solid polymer electrolyte (PSPE). The idea is that this combination can hold the liquid inside, and at the same time would have enough mechanical stability. This trapped liquid phase is key to achieving high ionic conductivities,[46] while the microporous polymer electrolytes maintain the high mechanical strength in this combined morphology.[47] As microporous porous solid electrolytes, PVdF and its copolymer PVdF-HFP have been studied vastly because of their promising characteristics. PVdF-HFP has more advantages than its homopolymer counterpart PVdF, for example, lower crystallinity, high solubility, and lower glass transition temperatures.[48,49] Therefore, for obvious reasons ILs have been combined with PVdF-HFP to benefit from their high ionic conductivity.[50] However, liquid retention ability of PVdF-HFP membranes is poor, and here excellent properties of PEO polymers come into play. The liquid retention of cross-linked polymers is much better than that of porous PVdF-HFP. The addition of PVdF-HFP was helpful to increase the pore size, porosity, and electrolyte uptake of the electrolyte membrane, which in turn increased the ionic conductivity of the polymer electrolyte.[51] This way, finally we have synthesized the semi-IPN polymer electrolyte composed of PVdF-HFP and cross-linked PEO, which shows successful liquid phase retention at higher temperature thanks to the electrostatic interaction between the PEO polymer and the lithium ions, while keeping suitable elasticity to withstand the mechanical stresses generated during lithium thermal deposition. In addition, it is worth mentioning that PVdF-HFP matrix helps improving high voltage

tolerance and prevents crystallization,[52] also the semi-IPN structure was found to help preventing "voltage noise" failure in an NMC622 | SPE | Li cell.[53]

Herein, semi-IPN gel electrolytes were prepared via a one-step method based on a thermal free radical polymerization of EGDMA (poly-ethyleneglycol dimethacrylate)/PEGM (polyethylene glycol methyl ether methacrylate) oligomers in the presence of PVdF-HFP, *N*-propyl-*N*-methylpyrrolidinium bis (fluorosulfonyl)imide ($P_{13}FSI$) and LiTFSI. A Li-metal microbattery prototype was demonstrated using this semi-IPN electrolyte (10 μm) with $LiCoO_2$ (LCO) as cathode and a thin layer of lithium as anode (10 μm) formed by thermal evaporation Such a semi-IPN electrolyte played the role of both electrolyte and separator in the thin-film based microbattery.

2. Results

2.1. Electrolyte Preparation and Microbattery Device Fabrication

Every mixture was prepared in terms of gravimetric ratio, *i.e.*, by measuring mass, which was measured by an OHAUS pioneer balance (accuracy of $\pm 10^{-4}$ g) at ambient temperature in a glove box (MBraun, with $[H_2O] < 1$ ppm, $[O_2] < 1$ ppm). Prior to the formulation of the gel polymer electrolyte, several mixtures of $P_{13}FSI$ with LiTFSI were made (which are grouped as 'Mixture A' – Figure 1a). In the process of making the series of 'Mixture A', LiTFSI was dissolved and stirred for one hour within $P_{13}FSI$, to prepare the 'mixture A', which is made of x mol L^{-1} LiTFSI in $P_{13}FSI$. Here x represents the molar concentration (mol per liter) of ionic liquid of the mixtures, with values of 0.6, 1, 1.3, 1.9, 2.8 and 3.2. Thereafter, every mixture was stored inside the argon-filled glove box to avoid contamination during the study. Using these mixtures, we formulated our semi-interpenetrated polymer network electrolyte (semi-IPN electrolyte), and also, we prepared another two types of electrolytes, in order to have a comparative optimization of the electrolyte parameters. The other two electrolytes are named depending upon the nature of the polymers inside (SI Table S1), while C-L electrolyte indicates a cross-linked polymer electrolyte and L electrolyte stands for a linear polymer electrolyte.

The three different types of gel electrolytes were prepared using the following process. At first, the preparation of the C-L electrolyte was carried out. As for the first step, thermal free radical polymerization of PEGDMA and PEGMA was done in the presence of AIBN (2 wt% of the monomers). PEGMA, PEGDMA and AIBN are miscible in 'mixture A'. Thus, to carry out the polymerization reaction, a mixture of PEGDMA, PEGMA and mixture A were prepared, which is called 'mixture B', as indicated in Figure 1b. After the dispense procedure (Figure 1c), the mixture was heated at 60 °C for 24 hours in an oven under vacuum to carry out the polymerization of PEGMA and PEGDMA. The resulting polymer electrolyte formed freestanding films, which were dry (Figure 1c). Thereafter, the L-electrolyte was prepared by drying PVdF-HFP in presence of acetone.

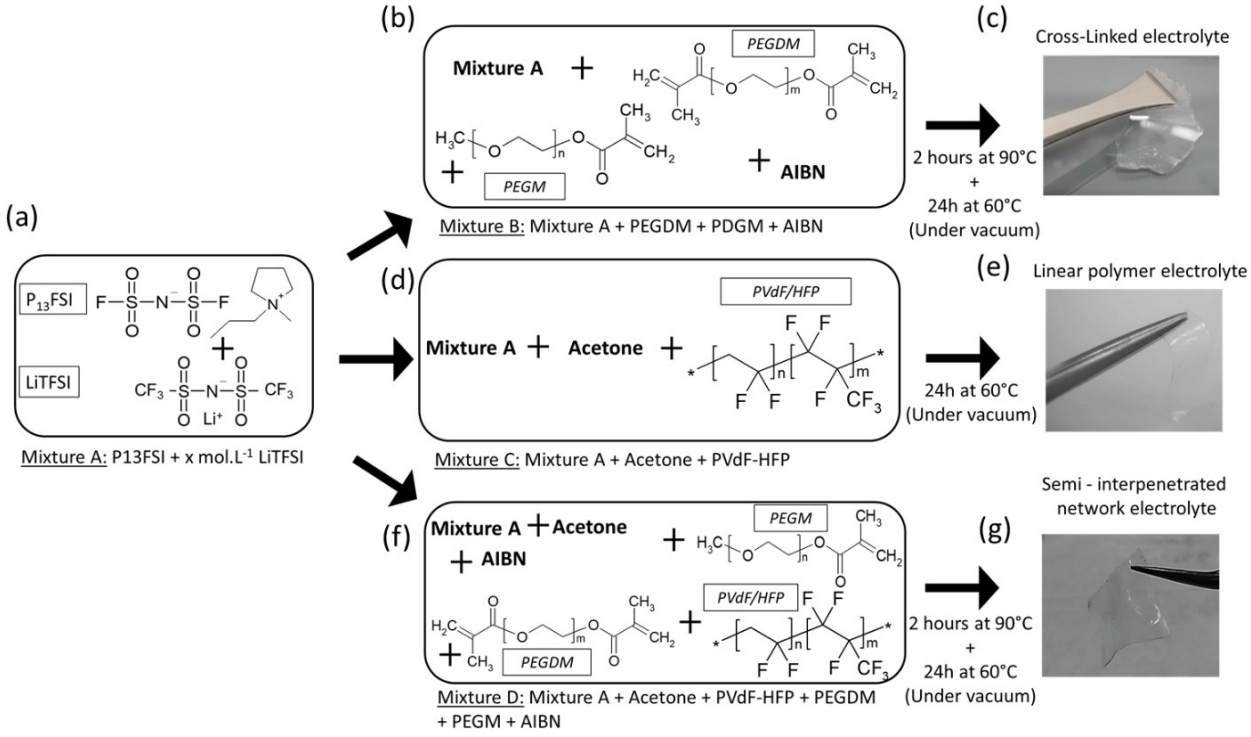

Figure 1. a) 'Mixture A': LiTFSI was dissolved and stirred for one hour within $P_{13}FSI$, to prepare the 'mixture A', which is *x* mol L^{-1} LiTFSI in $P_{13}FSI$. Here x represents concentrations of the mixtures, with values of 0.6, 1, 1.3, 1.9, 2.8 and 3.2. b) Preparation of mixture B (Mixture A + PEGDM + PDGM + AIBN). c) The cross-linked electrolyte. d) Preparation of 'mixture C' (Mixture A + Acetone + PVdF-HFP), e) the linear polymer electrolyte. f) Preparation of 'mixture D' (Mixture A + Acetone + PVdF-HFP + PEGDM + PDGM + AIBN), g) the semi-IPN electrolyte.

At first, PVdF-HFP was dissolved in acetone for 30 min then mixed with 'mixture A' to produce the so called 'mixture C' (Figure 1d).

After the dispense step (Figure 1e), the solution was dried at 60 °C for 24 hours inside an oven under vacuum. The resulting polymer electrolyte was a colorless transparent and free-standing film. Finally, the semi-IPN electrolyte was prepared as follows. The thermal free radical polymerization of PEGDMA and PEGMA, was done in the presence of AIBN (2 wt% of the monomers), with PVdF-HFP, in acetone solution. During the process, PVdF-HFP was first dissolved in acetone for a duration of 30 min, Thereafter, the resulting solution was mixed with 'mixture A', PEGDMA and PEGMA to prepare 'mixture D' (Figure 1f). Finally, the 'mixture D' was dispensed on a substrate (MICA, glass plate or $LiCoO_2$) to obtain a free-standing polymer electrolyte (Figure 1g).

In order to be compatible with thermal evaporation process, the semi-IPN polymer electrolyte was optimized for improved liquid electrolyte retention and crack prevention (with details in the following sections). The fabrication of the microbattery is depicted in Figure 2. At first, the polymer electrolyte was dispensed and dried/cured on the $LiCoO_2$ positive electrode. The positive electrode is an industry standard (component of EFL700 A39) consisting in a mica substrate and a platinum metal current collector, and a $LiCoO_2$ layer as a positive electrode, with a thickness of 10 μm (Figure 2a). Thereafter the gel polymer electrolyte layer was deposited on the positive electrode (Figure 2b). The thickness of the polymer electrolyte layer was determined with Bruker Dektak XT. The lithium negative electrode was deposited by thermal evaporation (Figure 2c) with a thickness of 10 μm (Figure 2h). The deposition was realized in a Plassys MEB400 reactor under controlled atmosphere in glove box ($[O_2] <$ 5 ppm; $[H_2O] < 5$ ppm; $[N_2] < 80$ ppm) to avoid contamination before and after deposition. To achieve the deposition, the lithium foil was cut and placed in a crucible inside the reactor. The lithium foil was heated between 500 to 600 °C by Joule effect at 2×10^{-7} mbar. The lithium was deposited at a 1 nm s^{-1} rate. To study comparative compatibilities, we also tried to deposit lithium on the other two type of electrolytes; and we failed to obtain a good quality of deposition of lithium on both types of C-L electrolyte (Figure S1b) and L electrolyte (Figure S1c). Excellent deposition quality of the thin layer of lithium metal was observed onto the semi-IPN electrolyte (Figure S1a). Schematic of the complete sandwiched structure of the microbattery is shown in Figure 2C, with its cross-section image in Figure 2e. The in-plane sandwich structure consisted of Li metal, deposited on top as negative electrode, a positive electrode at the bottom, and the gel polymer electrolyte in between. The photographs of the fabricated flexible device are shown in Figure 2d.

In parallel, a reference all solid-state device which is based on an inorganic electrolyte was prepared using a mica substrate, a platinum metal current collector, a $LiCoO_2$ (lithium cobalt oxide) layer as a positive electrode (stack provided by STMicroelectronics), a LiPON layer as a solid electrolyte and a lithium metal negative electrode. The overall thickness of the polymer electrolyte-based stack including other active parts (anode-cathode and electrolyte) is about 40 μm, with a 10 μm thick layer of LiPON electrolyte.

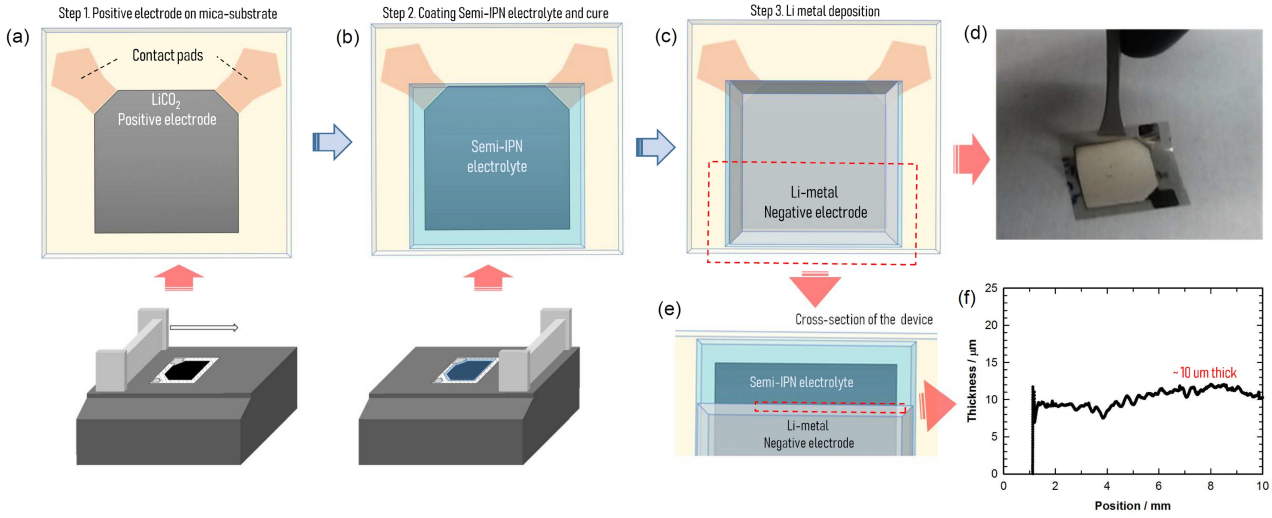

Figure 2. Schematic of the microbattery device: a) the positive electrode (industry standard, EFL700 A39); a mica substrate, a platinum metal current collector, and a LiCoO2layer with a thickness of 10 μm. b) A coating of gel polymer electrolyte was deposited on the positive electrode. c) Negative electrode (lithium metal) was deposited by thermal evaporation, and schematic of the complete sandwiched structure of the microbattery, with Li metal deposited on top, as the negative electrode, and the positive electrode is at the bottom, with the gel electrolyte sandwiched in between. d) Photographs of the real flexible device. e) A cross-section schematic of the device, f) thickness of the negative electrode (deposited lithium metal), and ~10 μm.

2.2. Optimization of the Ionic Liquid and Salt-Soaked GPE Matrices

2.2.1. Optimization of the Mechanical Properties of the GPE Matrices

In order to investigate the mechanical properties of the GPE matrices, static tensile tests were carried out using identical pieces of the resultant polymer electrolyte matrix. At first, the tests were performed on the matrix, made from the mixture of PVdF-HFP and the cross-linked PEO (DMA/MA = 4/1), and the results are shown in Figure 3a. Thereafter the effect of the electrolyte-intake (liquid phase intake within the polymer matrix) on the mechanical properties of GPE was analyzed (Figure 3b). A matrix, which was solely consisting of crosslinked based PEO (DMA/MA = 4/1) and had exhibited a poor mechanical strength (Figure 3a), with low values of elastic modulus E, and the strength and the elongation at break were found to be small.

It is worth mentioning that, for the cross-linked PEO based polymer, the value of the *E* module was equal to 2.2 MPa, which was much lower compared to that of 97.2 MPa for PVdF-HFP alone, i.e., PVdF-HFP had much higher rigidity than the POE based network. The formation of the PVdF-HFP-PEO matrix with different relative amounts of PVdF-HFP improves the elastic modulus. Increasing mass contents of PVdF-HFP, from 25, 50 to 75 wt%, increases the *E* modulus (from 4.9, 26.3 to 61.5 MPa respectively) and the breaking strength (1, 6 and 9 MPa respectively). Finally, we observed that the addition of PVdF-HFP increased the elongation at break up to 140% for a mass content of 75% compared to that of the elongation at break of the cross-linked PEO based polymer, which was limited to 1%. Thus, the incorporation of the PVdF-HFP in the PEO network improved the mechanical strength of the matrix significantly. Afterwards, effect of the encapsulation of liquid electrolyte (within the PVdF-HFP-PEO matrices) on the mechanical properties of the resultant matrix was studied. As expected, the encapsulated ionic liquid had played a plasticizer role, and reduced the interactions between the polymer chains.[26] As a result, we observed a reduction in Young's modulus of the resultant semi-IPN electrolyte matrix containing the entrapped liquid electrolyte. From the curves shown in Figure 3b and the data shown in Supporting Information Table S2, the addition of the electrolyte in the matrix reduced the stiffness of the material significantly. Indeed, by comparing the values of Supporting Information Table S2, we can see that, after introducing 80 wt% of liquid electrolyte, the Young's module E for the semi-IPN matrix decreased to a value of 2.6 MPa from 97.2 MPa for the PVdF-HFP alone. In addition, the elongation at break is increased by 80% with the addition of the liquid phase. Increasing the amount of PEO based network coupled with a decreasing amount of PVdF-HFP also caused decrease in stress and elongation at break. The encapsulation of the liquid phase by the polymer therefore lowered the modulus E and the stress at break; however, it improved elongation at break. These results confirm the plasticizing effect of the liquid phase on the polymer matrix, this character agreeing with the results obtained by DSC,[54] where we measured the glass transition temperature of a similar mixture without PVdF-HFP, and observed lowering of the glass transition temperature, T_g during the addition of the ionic liquid.

2.2.2. Measurements of Transport Properties of the GPE Matrices

The temperature dependance of the ionic conductivities were studied for all three type of electrolytes, i.e., the C-L, L- and semi-IPN electrolytes. The self-diffusion coefficients were also measured for all the ions present in all electrolytes. (Results are

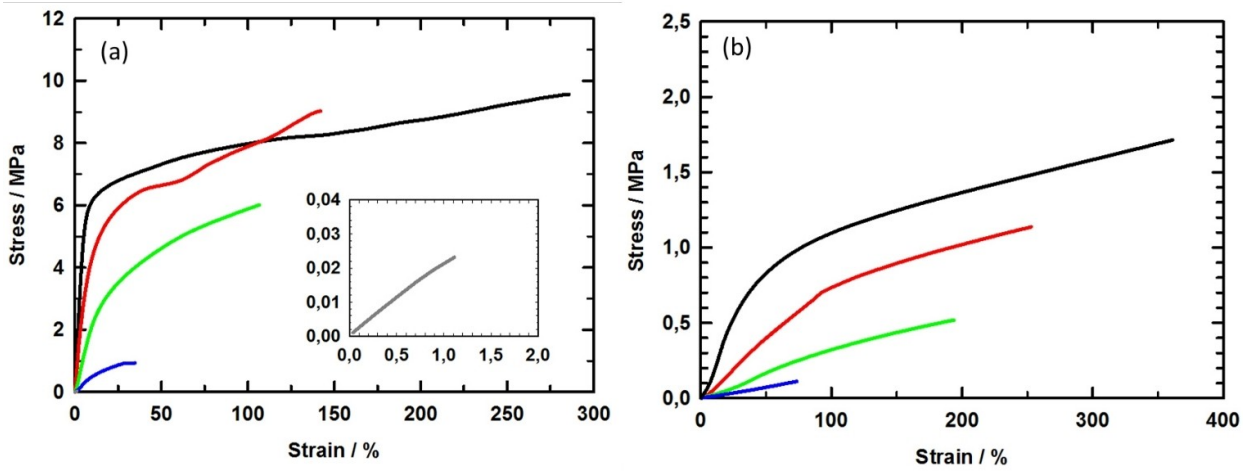

Figure 3. Static tensile tests for a) the electrolyte matrices without liquid encapsulation for following compositions; only PVdF-HFP (black), 75 wt% PVdF-HFP/25 wt% POE (red), 50 wt% PVdF-HFP/50 wt% POE (green), 25 wt% PVdF-HFP/75 wt% POE (blue), and only POE (grey). b) the electrolyte matrices with 80% liquid ($P_{13}FSI$ + 1 M LiTFSI) encapsulations for following compositions; 15 wt% PVdF-HFP/5 wt% POE (red) 10 wt% PVdF-HFP/10 wt% POE (green), 5 wt% PVdF-HFP/15 wt% POE (blue)

shown in Figure 4a and 4b). As expected, with the increase in the temperature, the ionic conductivities were higher irrespective of the electrolytes (Figure 4a). We can clearly see that the PVdF-HFP (L type) based electrolyte exhibits highest conductivity, and the lowest conductivity is observed for the cross-linked PEO (C-L type) electrolyte, whereas the semi-IPN electrolyte exhibited optimum properties and performances. Concerning the self-diffusion coefficients (Figure 4b), Pyr_{13}^{+}, $[TFSI]^{-}$ and $[FSI]^{-}$ diffuse almost at the same rates in all the three different electrolytes, indicating that there is no specific interaction is expected between these ions and the polymer phase. However, this is in stark contrast with Li^{+}, as it diffuses faster in the PVdF-HFP based electrolyte (L type) and it is considerably slowed down in the other two types of electrolytes.

The slowest diffusion for Li^{+} was observed for the PEO based C-L electrolyte, and an intermediate value was observed for semi-IPN electrolyte. The strong change in diffusion behavior for the PEO based C-L electrolyte seems to indicate that Li^{+} ions are often coordinated with the oxygen atoms of the less mobile polymer chains. This O–Li interactions within the polymer network adversely affect the Li^{+} ions' self-diffusion and will have an impact on the $^{7}Li^{+}$ relaxation behavior (vide infra).

For the semi-IPN electrolyte, the presence of PVdF-HFP improves Li^{+} self-diffusion: Li^{+} ions exhibited self-diffusion coefficients of $3.7\times10^{-12}\,m^{2}s^{-1}$ and $1.89\times10^{-13}\,m^{2}s^{-1}$ for the semi-IPN and the C-L electrolytes, respectively. The addition of the PVdF-HFP polymer within the cross-linked PEO polymer phase and decreases the number of O–Li interactions, directly improving Li^{+} ion diffusion. As shown in Figure 4c and 4d, the ^{7}Li longitudinal (T_1) and transverse relaxation times (T_2) were measured as function of the concentration of LiTFSI. The longitudinal relaxation time was found to have a mono-exponential dependency for all three type of electrolytes, whereas the transverse relaxation time exhibited bi-exponential behavior for the semi-IPN and C-L electrolytes, and mono-exponential behavior for the L type electrolyte. This bi-exponential dependency cannot be explained by the presence of two different types of lithiated species in the system, it is an intrinsic property of quadrupolar spins (^{7}Li has a spin S = 3/2, and therefore three single-quantum transitions hidden behind one single peak). Quadrupolar relaxation results usually from rapid fluctuations of the quadrupolar spin interaction, which itself is created by the fast motions occurring in the coordination sphere of the ion. Bi-exponential relaxation is usually observed when the fluctuations of the ^{7}Li spin environments are slowed down below a rate comparable to Larmor's

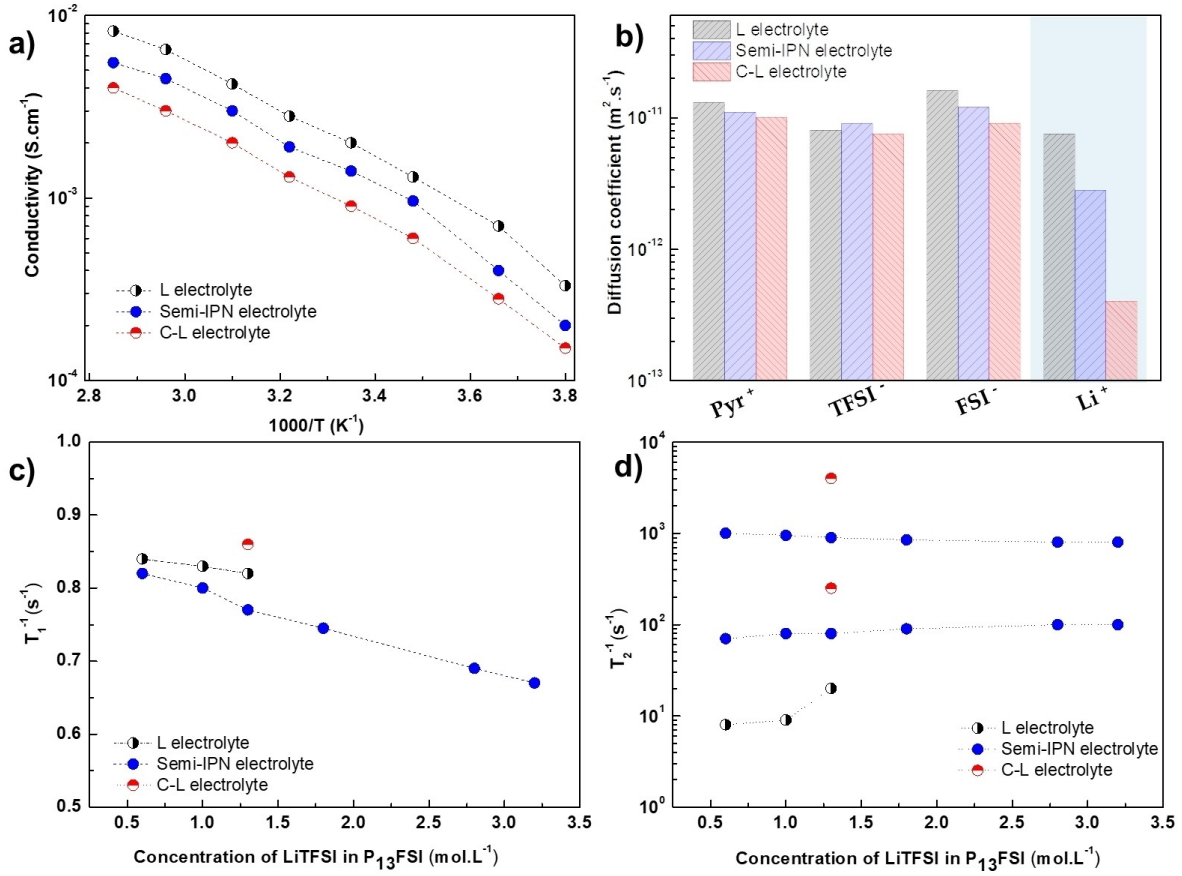

Figure 4. Transport properties of all three different type of electrolytes: L-type electrolyte; semi-IPN electrolyte; C-L type electrolyte. a) Dependency of the ionic conductivity as a function of the temperature. b) Ion diffusion coefficients at 33.5 °C. c) Longitudinal (T_1^{-1}) and d) transverse (T_2^{-1}) relaxation time constants of Li + as a function of the concentration

frequency (291 MHz here, i.e., fluctuations slow down to the 1–10 nanoseconds timescale), and the relaxation rates of the three 1-quantum spin transitions become different. In the case of fast fluctuations, we have a situation called "extreme narrowing", where the fluctuations occur on a much shorter timescale than the Larmor's period and all the transitions relaxation rates are the same (this is essentially the case in non-viscous liquid electrolytes). These results confirm the presence of interactions between oxygen (present in the slowly moving polymer chains) and Li^+ leading to a slowing down of the lithium motion and a rigidification of the lithium's immediate environment, confirming what was inferred from the decay of the lithium self-diffusion coefficient.[54]

2.2.3. Optimization of the Ionic Conductivities and Ion Diffusion Properties of the GPE Matrices

Figure 5a shows the changes in the ionic conductivity (at 25 °C) of the semi-IPN electrolyte as a function of the percentage of cross-linked PEO relative to the PVdF-HFP polymer within the electrolyte matrix. Higher proportions of cross-linked PEO caused a gradual decrease in ionic conductivity. Indeed, for a polymer phase consisting solely of PVdF-HFP, the conductivity reached 1.89×10^{-3} S cm^{-1}. The addition of 25%, 50% and 75% (weight percentage) of cross-linked PEO in the polymer phase lowered the conductivity to 1.22×10^{-3}, 1.02×10^{-3} and 0.95×10^{-3} S cm^{-1}, respectively. The increase of the crosslinked PEO phase lowered the mobility of the species by accentuating the interactions between the ions and the polymer chains.

This is in accordance with the NMR results, where we observed that Li^+ diffusion was the slowest for PEO based polymers and fastest for the PVdF-HFP based electrolyte, and an optimum was obtained for the semi-IPN based electrolyte. In the PEO based polymers, we observed interaction between Li^+ ions, and oxygen within the PEO, and this interaction can hold back Li^+ ions, giving rise to the bi-exponential of relaxation behavior. Figure 5b shows how the concentrations of the LiTFSI salt influence the conductivity of the semi-IPN electrolyte matrix. For this study, the semi-IPN electrolyte matrix consisted of PVdF-HFP (15 wt%) and PEO based polymer (5 wt%) with 80 wt% of '*x*' mol L^{-1} LiTFSI in P_{13}FSI, with '*x*' between 1.0 to 1.9 was studied. As expected, increasing the concentration of LiTFSI salt lowers the ionic conductivity. The ionic conductivity decreased from 1.22×10^{-3} to 0.84×10^{-3} S cm^{-1} for a concentration change from 1.0 to 1.9 mol L^{-1},

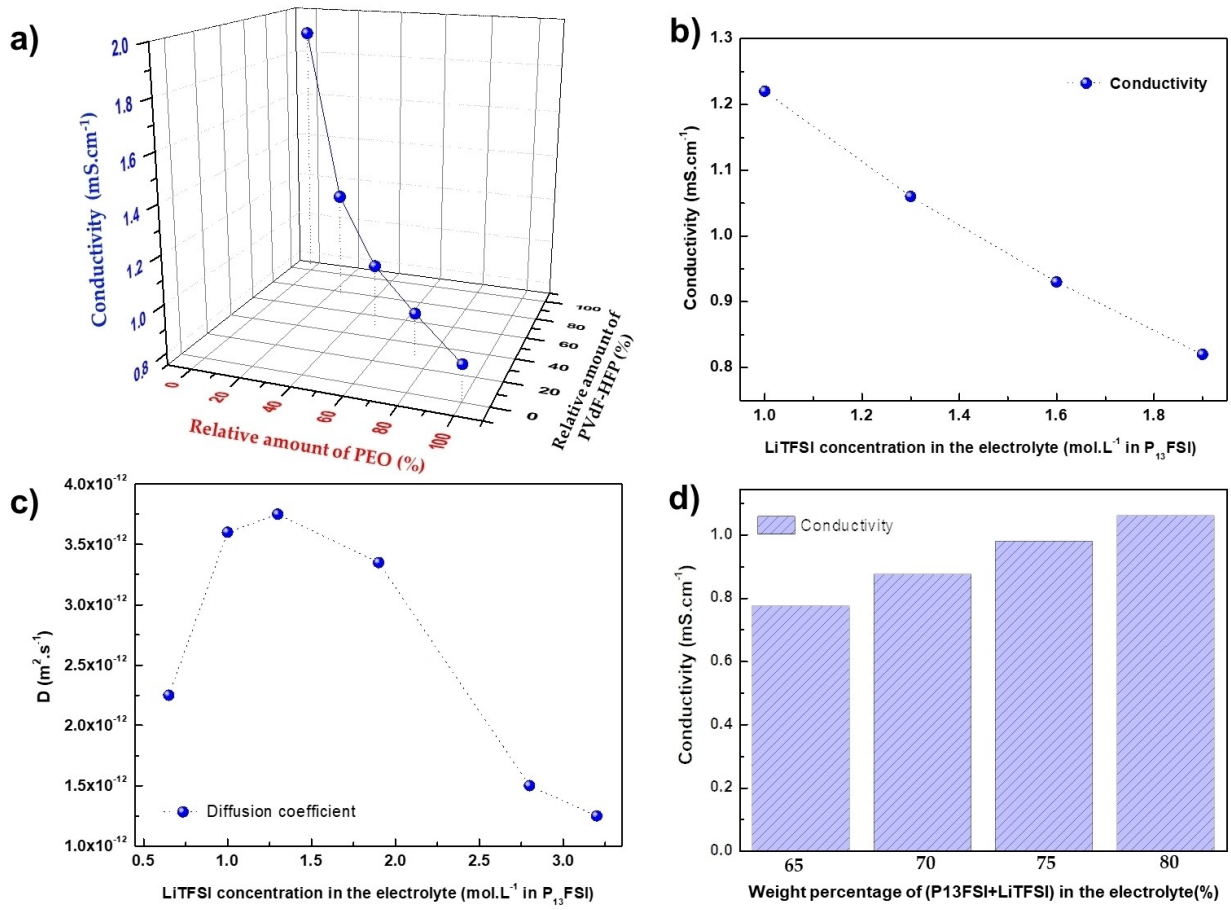

Figure 5. a) Changes in the ionic conductivity (at 25 °C) of the semi-IPN electrolyte as a function of the percentage of cross-linked PEO relative to the PVdF-HFP polymer within the electrolyte matrix. b) Dependency of the concentrations of the LiTFSI salt and the conductivity of the semi-IPN electrolyte matrix, c) diffusion coefficient of Li + as a function of the LiTFSI concentrations. d) Dependency of the conductivity on the relative weight percentage of (P_{13}FSI + LiFSI) in the electrolyte.

and this result can be attributed to the increase of the viscosity and ions pairing in the mixture.[36] The diffusion coefficient of Li^+ was measured as a function of the LiTFSI concentration, which was varied over a wide range from 0.1 to 3.2 mol L^{-1} (Figure 5c). It was observed that the self-diffusion coefficient of Li^+ increased up to a concentration of 1.3 mol $L^{-1,}$ and thereafter decreased continuously between 1.3 and 3.2 mol L^{-1}. Initially, for a low concentration of LiTFSI, most of the Li^+ ions in the system are expected to be coordinated with the numerous oxygens of the PEO polymer, resulting in the initial slowdown of the lithium-ion diffusion. However, increasing the Li^+/O ratio is expected to reduce the Li-O interactions effect, as the weight of the pool of free ions increases, and fast exchange between bound and free lithium ions will lead to all lithium ions spending more time within the porosity of the electrolyte. This phenomenon was observed until up to a concentration of 1.3 mol L^{-1}. Beyond this concentration, the viscosity of the liquid electrolyte becomes predominant, as a result, it slows lithium self-diffusion down. With this result, the concentration of LiTFSI in the liquid phase of semi-IPN electrolyte was set at 1.3 mol L^{-1}. Figure 5d displays the conductivity of the electrolyte matrix as a function of the relative liquid-phase ($P_{13}FSI$ + LiTFSI) content of the composite matrix. We can clearly see that the conductivity increases with the relative amount of liquid phase. Based on all these observations, the composition with 5 wt% cross-linkable PEO, 15 wt% PVdF-HFP and 80 wt% of liquid electrolyte (i.e., a mixture of 1.3 mol L^{-1} LiTFSI in $P_{13}FSI$) was chosen as an optimal composition combining optimal transport properties and good mechanical properties.

Each component of the composite GPE electrolyte played crucial role in obtaining the final stable electrolyte with unique mechanical properties. The mixture of PVdF-HFP with crosslinked PEO provided an optimum blend of polymers. The PVdF-HFP offered excellent mechanical stability and at the same time good lithium-ion conductivity through its porosity. In comparison to other two types of electrolytes, PVdF-HFP (L-type) provided the largest diffusion coefficients for Li^+, thanks to the ion conducting channels through the porosity of the structure, and the fact that Li^+ ions are coordinated only with the anions of the ionic liquid. Thanks to this porosity, the IL can swell in the pores very easily and have the high conductivity through the pores without any hindrance. On the other hand, the presence of PEO polymer, which was blended in the matrix, improved the liquid retention capacity, and provided drastic improvement in liquid encapsulation, thanks to the electrostatic interactions between the Li^+ ions and the PEO polymer. Without crosslinked PEO, the poor liquid retention capacity of PVdF-HFP makes them vulnerable at higher temperatures (60°C), and liquid spills out. The semi-IPN blend provided excellent liquid retention, as well as good mechanical stability and flexibility. However, the conductivity of the polymer matrix decreased for with higher proportions of the PEO based network, because of the increased interactions between the Li ions and oxygen atoms of the PEO polymer chain. However, thanks to the liquid component of the electrolyte, conductivity remains reasonably high. Here, we observed that 1.3 M was the optimum concentration. In the system, a portion of Li^+ ions can be coordinated with the oxygen atoms of the PEO network, and this slows down the diffusions. However, higher concentrations lead to an increase in the number of free lithium ions (which are not coordinated with oxygens of PEO), and a higher conductivity. On the other hand, for concentrations over 1.3 M, viscosity increased and slowing down the diffusion of all ions.

Finally, it is worth mentioning that, the final GPE was very stable electrochemically, which was again confirmed by our observations of negligible resistance changes during EIS measurements from Li/electrolyte/Li full cell configuration (Figure S1 in the Supporting Information).

2.3. Electrochemical Performance of the Microbattery

We first tested electrochemical stability window for the semi-IPN electrolyte, and we found a value of more than 4.7 V (Figure S2). Thereafter, we tested the electrochemical performance of our microbattery with semi-IPN electrolyte (Figure 6a), and compared it with that of the reference device, which we fabricated. (Figure 6b).

For both, we can see three charge-discharge curves, which were obtained at C/2, C and 2C charge-discharge rates. It is evident that, with increasing C-rates, the retention of the capacity of the reference device turned out to be poorer compared to that of our semi-IPN based microbattery. The semi-IPN based microbattery retained more than 80% and 70% of the initial capacities upon charging at C and 2C, respectively. In contrast, for the reference device, retention of capacity was dropped down to an extremely poor value of 32% at 2 C, whereas around 72% retention was observed for the 1C charging rate. With increasing charging speed, failure in the retention of capacity of the reference microbattery can be attributed to the poor ionic conductivity of the LiPON (10^{-6} S cm^{-1} at 30 °C) which induces a high internal resistance. Not only that, as LiPON is a solid-state electrolyte, it exhibits highly resistive electrode/electrolyte interfaces,[8,9] which is a hindrance for higher current, and it negatively affects good retention of the capacity at higher charging speeds. Whereas semi-IPN based microbattery can achieve a faster lithium charge transport within the liquid components of the gel-polymer electrolyte matrix. A liquid electrolyte (1.3 mol L^{-1} LiTFSI in IL) has much lower resistance compared to that of solid substance of the LiPON inorganic electrolytes, and thus provides much faster charge/discharge performances. This non-fluidic nature of the solid-state electrolyte inherently limits the contact area between the electrode surface and solid electrolyte. This issue is better addressed when a polymer electrolyte with softer mechanical properties is introduced. Here, our semi-IPN electrolyte plays a very important role because of its soft polymer material properties, which creates better interface, minimizing interfacial resistance at the electrode/electrolyte interface.[10] In addition, more fluidic nature of an electrolyte ensures a better wettability of the electrode porosity. These two phenomena greatly influence the overall polarization of an electrode, and higher polarization was observed for larger contact resistance and hence for the LiPON electrolyte. As a

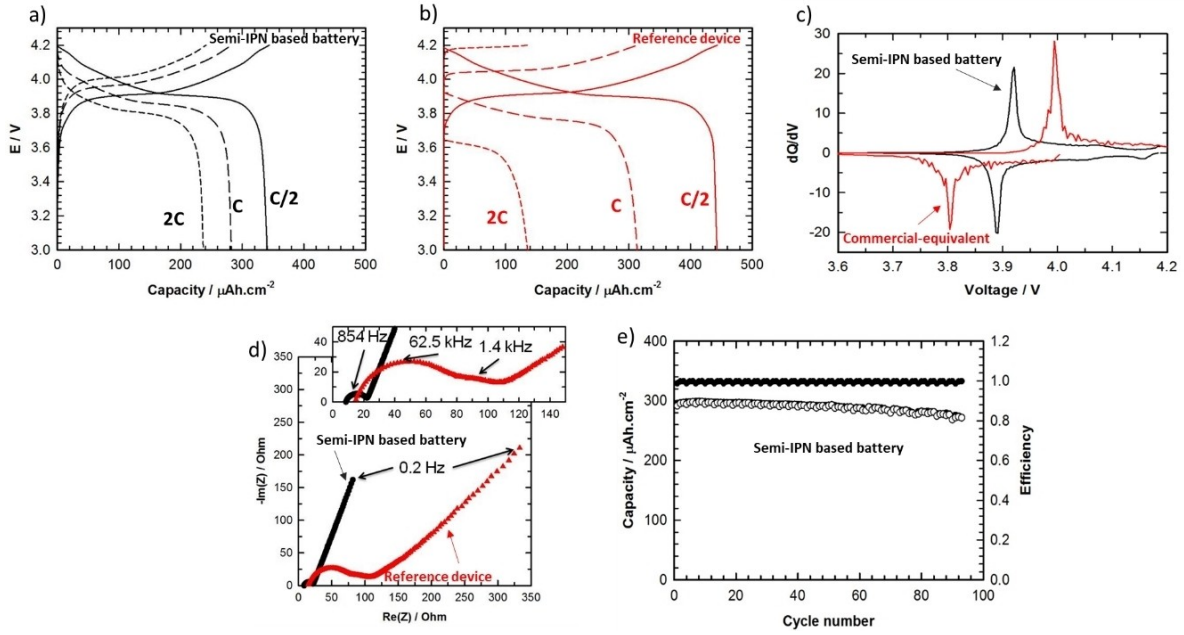

Figure 6. Charge–discharge curves of a) our microbattery with semi-IPN electrolyte and b) the reference battery at different charge-discharge rates (C/2, C and 2 C). c) Differential changes in the stored charges in the battery systems, with respect to the changes in the voltages. d) Nyquist plots for both devices and e) cyclic stability with coulombic efficiency of the semi-IPN electrolyte based microbattery.

result, we observed relatively larger drops in the discharge plateau potentials with increased charging speeds for the LiPON based commercial-equivalent microbattery, compared to that of our semi-IPN based device. The discharge plateaus for the commercial-equivalent microbattery dropped from 3.9 V to 3.6 V (300 mV) when discharging it at 2C instead of C/2, while the semi-IPN based device displays a voltage drop of 100 mV, from 3.9 V to 3.8 V. Figure 6c shows differential changes in the stored charges in the battery systems, with respect to the changes in the voltages. We can clearly see a wider shift in the peaks position for the LiPON electrolyte, which is in well agreement with the expected higher polarization due to the lower conductivity and poorer interfaces the case of LiPON based reference battery. The limited ionic conductivity and higher polarization issues of the LiPON electrolyte were further confirmed by the Nyquist plot (Figure 6d) obtained with electrochemical impedance spectroscopy. We can clearly see from the lower frequency region (0.2 Hz) that higher diffusion difficulties were observed for the only for PVdF-HFP based electrolyte, compared to semi-IPN based electrolyte. Whereas higher frequency region indicates higher ESR values, implying higher overall resistance of the system, including internal and contact resistances. We have also carried out compatibility tests for both electrolytes with the lithium metal in a Li/electrolyte/Li full (both the positive and negative electrodes were Li metals). The evolution of the cell impedance has been depicted in Figure S3 in the supporting information. From this result one can conclude that the semi-IPN electrolyte exhibits lower reactivity toward lithium metal. Indeed, there is a large change in the impedance for the case of PVdF based electrolytes compared to that was obtained for semi-IPN based electrolytes. This large change in the resistance represents presence of some chemical reaction, indicating instability for the case of PVdF based electrolytes. Figure 6e represents cyclic stability and the efficiency of our microbattery, and we can see an excellent stability over 100 cycles, with almost 100% efficiency.

3. Discussion

Thanks to this optimized self-standing structure, and associated mechanical stabilities, we could use direct deposition techniques such as the thermal evaporation on the surface of GPE embedding liquid electrolyte inside. This liquid part not only improved the ionic conductivity of the GPE system, but also played an important role as : first, a wetting agent at the interface between the solid electrode and the GPE electrolyte, second, the liquid component can be extremely useful in filling the voids at the interface of the micro-battery system.[56] Here, it is worth mentioning that, this self-supporting GPE is very tricky to obtain. In another reported case, (in situ free radical co-polymerization of polyethylene glycol dimethacrylate and polyethylene glycol methyl ether methacrylate in a (1-methyl-1-propylpyrrolidinium bis(trifluoromethylsulfonyl)imide (P_{13}TFSI) + LiTFSI) mixture), a similar GPE was obtained, with good conduction properties, but failed to provide self-sustaining structure and required a support of cotton mesh to achieve the structural stability, before being used as a separator.[57] In other reported works, self-sustaining polymer electrolytes were obtained via free radical polymerization technique, however lithium foils were used to assemble full cell configurations.[58,59]

Therefore, in our case, the resultant GPE is strong enough to form a self-standing thin film, able to hold the liquid inside without any leakage, preventing lithium dendrite formation

during cycling, and displaying chemical and physical stability enabling it to withstand the metal deposition stress.

Additionally, we must highlight the advantages of our approach, where all the polymer precursors used in our process were liquids. The benefits of such starting materials are enormous, such as, these precursors, being in the liquid state, are compatible with many standard and low-cost techniques. Spray coating, inkjet, or screen-printing drop casting processes can be easily used to deposit the electrolyte film and the polymerization step can also be achieved by simple techniques like ultraviolet (UV)-cures.[14] In standard practice, the above mentioned techniques may lead to poor mechanical properties of the resultant polymer, which can either be too soft (no firm shape) or too rigid (a liquid electrolyte-soaked layer might be required to reduce polarizations at the interface).[60] For polymers which are too soft, there would be requirement for supports through external packing,[1] and/or covers with materials like polyacrylate during device fabrication.[15] In contrast, our semi-IPN electrolyte, thanks to its quasi-solid state and excellent mechanical properties, acted as both separator and electrolyte in a self-standing form without any additional packaging, and also provided optimal lithium-ion diffusivity at 1.3 mol L^{-1} of LiTFSI. Optimum ion diffusivity reduces the impact of the concentration polarization thus decreasing cell polarization. The nominal voltage and the capacity of the battery are therefore higher by comparison to the LIPON based micro-battery. It is also worth noticing that the reported performances and the stability up to 100 cycles have been obtained with a directly deposited lithium thin-film anode of only 10 microns thick while most of reported studies used lithium foil anodes of several hundreds of microns.[60,15,16] Keeping in mind that lithium anode has been directly deposited on the backside of the electrolyte, the results obtained herein can be considered as very promising and could open the way to new methods and strategies in preparing lithium metal-based microbatteries.

4. Conclusions

We prepared and optimized semi-IPN GPE matrix, made of a composite containing 5 wt% of cross-linkable PEO, 15 wt% of PVdF-HFP and 80 wt% of the liquid electrolyte at 1.3 mol L^{-1} of LiTFSI in $PYR_{13}FSI$. The self-supporting film displayed a good mechanical strength and a quasi-solid structure with excellent liquid retention capacity. The transport properties of this semi-IPN electrolyte were measured as function of concentration of LiTFSI salt, and longitudinal (T_1) and transverse relaxation times (T_2) were determined using Nuclear magnetic resonance (NMR) analysis. A bi-exponential dependency of the time constants was observed, which indicated interactions between Li-ions and oxygens within the polymers. This interaction played a key role to balance between the lithium-ion diffusion and the polymer matrix liquid retention capacity. The optimum composition of the polymers was the key in determining physical properties of the resultant electrolyte, including its promising conductivities, flexibility, and absence of liquid leakage. Moreover, the semi-IPN based electrolyte gives comparatively much better mechanical strength compared to above mentioned other GPEs, and that made it possible to integrate processes like thermal evaporation, for lithium deposition. This makes it the first ever polymer-based electrolyte reported so far, that is compatible with such techniques. Moreover, the resulting device displays a lower impedance, and a higher nominal voltage retention at fast discharging rates, a better capacity at fast recharging rates, an outstanding capacity and cycling stability with high reversibility, and therefore it holds more promise in comparison to conventional available LiPON and other ceramics or even other developed GPE based micro-batteries.

Experimental Section

Materials

Poly (vinylidene fluoride-co-hexafluoropropylene) (PVdF-HFP, Solef 21216) was purchased from Solvay. Radical initiator 2, 2′-azobis (2-methylpropionitrile) (AIBN, 98%, [CAS]: 78-67-1), poly-(ethyleneglycol) dimethacrylate (PEGDMA, Mn: 550, [CAS]: 25852-47-5) and poly (ethyleneglycol) methyl ether methacrylate (PEGMA, Mn: 500, [CAS]: 26915-72-0) were obtained from Sigma Aldrich. Anhydrous acetone was acquired from VWR (max. 0.01% H_2O, [CAS]: 67-64-1). AIBN was purified by recrystallization in methanol before its use. PEGMA, PEGDMA, PVdF-HFP and AIBN were dried at 40 °C under vacuum for five days and stored in a glove box until its usage (MBraun, with H2O < 1 ppm, O2 < 1 ppm). Lithium bis [trifluoromethylsulfonyl]imide, (LiTFSI, 99.9%, [H_2O] < 20 ppm, [CAS]: 90076-65-6) and the room temperature ionic liquid (RTMS) 1-propyl-1-methylpyrrolidinium bis(fluorosulfonyl)imide ($P_{13}FSI$, 99.9%, H2O < 20 ppm, [CAS]: 852620-97-4) were obtained from Solvionic and stored under nitrogen atmosphere (MBraun, with [H_2O] < 1 ppm, [O_2] < 1 ppm) to avoid any moisture contamination. They were used as received without further purification.

Measurements and Characterizations

The ionic conductivities of the electrolytes were measured using electrochemical impedance Spectroscopy. The samples were placed between two Pt blocking electrodes (2 cm^2) in a symmetrical cell (coin cell, CR 2032). Then the Nyquist plots were recorded between 500 kHz and 5 mHz at 25 °C in potentiostatic mode with a perturbation amplitude of 10 mV.

Pulse-field gradient stimulated echo (PFG-STE) diffusion measurements were realized on a Bruker 750 MHz wide bore spectrometer, equipped with a Micro 2.5 gradient system and a 1H-19F/31P-17O double resonance 3.2 mm Magic Angle Spinning Bruker probe. The diffusion coefficient of the pyrrolidinium cation (1H) and of the bis (fluorosulfonyl)imide anion (19F) were measured using a stimulated echo sequence,[33] with a diffusion delay Δ, between gradient pulses around 20–100 ms and sine-shaped gradient pulses of effective duration δ, between 1 and 5 ms depending upon the diffusion coefficient measured. Sixteen data points of gradient values were used, and the echo decay was fitted with the Stejskal-Tanner equation to retrieve the self-diffusion coefficient. The longitudinal relaxation times (T_1) were measured with a saturation recovery experiments, using various relaxation delays between 10 µs and 10 s. The transverse relaxation times (T_2) were measured with a standard Hahn echo sequence, using echo durations between 10 µs and 500 ms. The relaxation delays were set to

5 seconds to ensure quantitative measurements for the diffusion and T_2 experiments. All samples were packed in a 3.2 mm NMR rotor inside an Ar filled glovebox. Field Emission Scanning Electron Microscopy (FE-SEM) was performed in a Zeiss ULTRA plus microscope.

The compatibility with thermal evaporation (of lithium metal) process was conducted with a sample of 10 μm thick of polymer electrolyte, dispensed and cured on mica substrate with a platinum current collector. 10 μm of metallic lithium was deposited on the polymer electrolyte. The resulting sample was visually compared with a reference sample. An OCV measurement was realized to confirm the absence of short-circuit.

The electrochemical tests were conducted on the microbattery configuration and the performances were compared with a reference device, which was fabricated with the similar configuration of a commercial microbattery (the process is described in later section). The electrochemical characterization of the microbatteries was conducted using constant current of charge and discharge (C/20 = 50 μA; C = 1.0 mA) with a cut-off voltage of 3.0 V (end of discharge) and 4.2 V (end of charge) in Li/$LiCoO_2$ microbatteries. Electrochemical Impedance Spectroscopy (EIS) measurements of the Li/$LiCoO_2$ microbatteries were performed at the open circuit voltage between 500 kHz and 5 mHz with perturbation amplitude of 10 mV. All electrochemical measurements were carried-out at 25 °C on a Versatile Multichannel Potentiostat (Biologic S.A.).

Acknowledgments

STMicroelectronics, the Region Centre Val de Loire and "Le Studium Loire Valley Institute for Advanced Studies" are gratefully acknowledged for financial support to researchers involved in this study.

Conflict of Interest

The authors declare no conflict of interest.

Keywords: Li-ion battery · microbattery · gel polymer electrolyte · ionic liquid · solid-state battery

[1] S. Ferrari, M. Loveridge, S. D. Beattie, M. Jahn, R. J. Dashwood, R. Bhagat, *J. Power Sources* **2015**, *286*, 25–46.
[2] F. Gu, J. Niu, L. Jiang, X. Liu, M. Atiquzzaman, *J. Netw. Comput. Appl.* **2020**, *149*, 102459.
[3] K. Kanehori, K. Matsumoto, K. Miyauchi, T. Kudo, *Solid State Ionics* **1983**, *9–10*, 1445–1448.
[4] G. Meunier, R. Dormoy, A. Levasseur, *MAT SCI ENG B-ADV.* **1989**, *3*, 19–23.
[5] J. Bates, *Solid State Ionics* **1992**, *53–56*, 647–654.
[6] J. B. Bates, N. J. Dudney, G. R. Gruzalski, R. A. Zuhr, A. Choudhury, C. F. Luck, J. D. Robertson, *J. Power Sources.* **1993**, *43*, 103–110.
[7] B. Wang, J. B. Bates, F. X. Hart, B. C. Sales, R. A. Zuhr, J. D. Robertson, *J. Electrochem. Soc.* **1996**, *143*, 3203.
[8] N. Ohta, K. Takada, I. Sakaguchi, L. Zhang, R. Ma, K. Fukuda, M. Osada, T. Sasaki, *Electrochem. Commun.* **2007**, *9*, 1486–1490.
[9] N. Ohta, K. Takada, L. Zhang, R. Ma, M. Osada, T. Sasaki, *Adv. Mater.* **2006**, *18*, 2226–2229.
[10] H. Kitaura, A. Hayashi, T. Ohtomo, S. Hama, M. Tatsumisago, *J. Mater. Chem.* **2011**, *21*, 118–124.
[11] P. Hu, Y. Duan, D. Hu, B. Qin, J. Zhang, Q. Wang, Z. Liu, G. Cui, L. Chen, *ACS Appl. Mater. Interfaces.* **2015**, *7*, 8, 4720–4727.
[12] S.-Y. Shen, R.-X. Dong, P.-T. Shih, V. Ramamurthy, J.-J. Lin, K.-C. Ho, *ACS Appl. Mater. Interfaces.* **2014**, *6*, 21, 18489–18496.
[13] Q. Chen, R. Xu, Z. He, K. Zhao, L. Pan, *J. Electrochem. Soc.* **2017**, *164*, A1852.
[14] F. N. Crespilho, G. C. Sedenho, D. de Porcellinis, E. Kerr, S. Granados-Focil, R. G. Gordon, M. J. Aziz, *J. Mater. Chem. A.* **2019**, *7*, 24784–24787.
[15] A. T. Kutbee, R. R. Bahabry, K. O. Alamoudi, M. T. Ghoneim, M. D. Cordero, A. S. Almuslem, A. Gumus, E. M. Diallo, J. M. Nassar, A. M. Hussain, N. M. Khashab, M. M. Hussain, *npj Flex.Electron.* **2017**, *1*, 7.
[16] H. Porthault, C. Calberg, J. Amiran, S. Martin, C. Páez, N. Job, B. Heinrichs, D. Liquet, R. Salot, *J. Power Sources.* **2021**, *482*, 229055.
[17] X. Wang, Z. Liu, C. Zhang, Q. Kong, J. Yao, P. Han, W. Jiang, H. Xu, G. Cui, *Electrochim. Acta.* **2013**, *92*, 132–138.
[18] J. Kalhoff, G. G. Eshetu, D. Bresser, S. Passerini, *ChemSusChem.* **2015**, *8*, 2154–2175.
[19] I. Osada, H. de Vries, B. Scrosati, S. Passerini, *Angew. Chem. Int. Ed.* **2016**, *55*, 500–513; *Angew. Chem.* **2016**, *128*, 510–523.
[20] A. M. Christie, S. J. Lilley, E. Staunton, Y. G. Andreev, P. G. Bruce, *Nature.* **2005**, *433*, 50–53.
[21] Y. Zhu, F. Wang, L. Liu, S. Xiao, Z. Chang, Y. Wu, *Energy Environ. Sci.* **2013**, *6*, 618–624.
[22] A. Manuel Stephan, *Eur. Poly. J.* **2006**, *42*, 21–42.
[23] C. M. Mathew, K. Kesavan, S. Rajendran, *Polym. Int.* **2015**, *64*, 750–757.
[24] Y. Zhu, S. Xiao, Y. Shi, Y. Yang, Y. Hou, Y. Wu, *Adv. Energy Mater.* **2014**, *4*, 1300647.
[25] D. E. Fenton, J. M. Parker, P. V. Wright, *Polymer.* **1973**, *14*, 589.
[26] P. Yao, H. Yu, Z. Ding, Y. Liu, J. Lu, M. Lavorgna, J. Wu, X. Liu, *Frot. Chem.* **2019**, *7*, 522.
[27] Y. Dkhissi, F. Huang, Y.-B. Cheng, R. A. Caruso, *J. Phys. Chem. C.* **2014**, *118*, 30, 16366–16374.
[28] J. Rolland, J. Brassinne, J.-P. Bourgeois, E. Poggi, A. Vlad, J.-F. Gohy, *J. Mater. Chem. A.* **2014**, *2*, 11839–11846.
[29] P.-L. Kuo, C.-A. Wu, C.-Y. Lu, C.-H. Tsao, C.-H. Hsu, S.-S. Hou, *ACS Appl. Mater. Interfaces.* **2014**, *6*, 3156–3162.
[30] R. Bouchet, S. Maria, R. Meziane, A. Aboulaich, L. Lienafa, J.-P. Bonnet, T. N. T. Phan, D. Bertin, D. Gigmes, D. Devaux, R. Denoyel, M. Armand, *Nat. Mater.* **2013**, *12*, 452–457.
[31] S. Song, Y. Wu, W. Tang, F. Deng, J. Yao, Z. Liu, R. Hu, Alamusi, Z. Wen, L. Lu, N. Hu, *ACS Sustainable Chem. Eng.* **2019**, *7*, 7163–7170.
[32] Q. Guo, Y. Han, H. Wang, S. Xiong, W. Sun, C. Zheng, K. Xie, *J. Phys. Chem. C* **2018**, *122*, 10334–10342.
[33] P.-E. Delannoy, B. Riou, T. Brousse, J. le Bideau, D. Guyomard, B. Lestriez, *J. Power Sources.* **2015**, *287*, 261–267.
[34] A. Noda, K. Hayamizu, M. Watanabe, *J. Phys. Chem. B.* **2001**, *105*, 4603–4610.
[35] H. Tokuda, K. Hayamizu, K. Ishii, Md. A. B. H. Susan, M. Watanabe, *J. Phys. Chem. B.* **2005**, *109*, 6103–6110.
[36] T. Niitani, M. Amaike, H. Nakano, K. Dokko, K. Kanamura, *J. Electrochem. Soc.* **2009**, *156*, A577.
[37] G. B. Appetecchi, S. Scaccia, C. Tizzani, F. Alessandrini, S. Passerini, *J. Electrochem. Soc.* **2006**, *153*, A1685.
[38] D. R. MacFarlane, J. Huang, M. Forsyth, *Nature.* **1999**, *402*, 792–794.
[39] Y. Cheng, L. Zhang, S. Xu, H. Zhang, B. Ren, T. Li, S. Zhang, *J. Mater. Chem. A.* **2018**, *6*, 18479–18487.
[40] S. Wang, Q. X. Shi, Y. S. Ye, Y. Xue, Y. Wang, H. Y. Peng, X. L. Xie, Y. W. Mai, *Nano Energy.* **2017**, *33*, 110–123.
[41] C. Gerbaldi, J. R. Nair, S. Ferrari, A. Chiappone, G. Meligrana, S. Zanarini, P. Mustarelli, N. Penazzi, R. Bongiovanni, *J. Membr. Sci.* **2012**, *423–424*, 459–467.
[42] J. R. Nair, L. Porcarelli, F. Bella, C. Gerbaldi, *ACS Appl. Mater. Interfaces* **2015**, *7*, 23, 12961–12971.
[43] F. González, P. Tiemblo, N. García, O. Garcia-Calvo, E. Fedeli, A. Kvasha, I. Urdampilleta, *Membranes* **2018**, *8*, 55.
[44] E. Simonetti, M. Carewska, G. Maresca, M. de Francesco, G. B. Appetecchi, *J. Electrochem. Soc.* **2017**, *164*, A6213.
[45] D. Zhou, D. Shanmukaraj, A. Tkacheva, M. Armand, G. Wang, *Chem.* **2019**, *5*, 2326–2352.
[46] S. W. Choi, S. M. Jo, W. S. Lee, Y.-R. Kim, *Adv. Mater.* **2003**, *15*, 23, 2027–2032.
[47] A. Manuel Stephan, K. S. Nahm, *Polymer.* **2006**, *47*, 5952–5964.
[48] J.-M. Tarascon, A. S. Gozdz, C. Schmutz, F. Shokoohi, P. C. Warren, *Solid State Ionics* **1996**, *86–88*, 49–54.
[49] P. Kubisa, *J. Polym. Sci. Part A* **2005**, *43*, 20, 4675–4683.

[50] N. H. Idris, Md. M. Rahman, J.-Z. Wang, H.-K. Liu, *J. Power Sources.* **2012**, *201*, 294–300.
[51] S. J. Dillon, K. Wook Noh, *Microsc. Microanal.* **2014**, *20*, 330–337.
[52] H. Fan, C. Yang, X. Wang, L. Liu, Z. Wu, J. Luo, R. Liu, *J. Electroanal. Chem.* **2020**, *871*, 114308.
[53] G. Homann, L. Stolz, K. Neuhaus, M. Winter, J. Kasnatscheew, *Adv. Funct. Mater.* **2020**, *30*, 2006289.
[54] V. Chaudoy, F. Ghamouss, E. Luais, F. Tran-Van, *Ind. Eng. Chem. Res.* **2016**, *55*, 37, 9925–9933.
[55] T. V. Huynh, R. J. Messinger, V. Sarou-Kanian, F. Fayon, R. Bouchet, M. Deschamps, *J. Chem. Phys.* **2017**, *147*, 134902.
[56] S. A. Pervez, G. Kim, B. P. Vinayan, M. A. Cambaz, M. Kuenzel, M. Hekmatfar, M. Fichtner, S. Passerini, *Small.* **2020**, *16*, 14, 2000279.
[57] C. Liao, X.-G. Sun, S. Dai, *Electrochim. Acta.* **2013**, *87*, 889–894.
[58] M. Falco, L. Castro, J. R. Nair, F. Bella, F. Bardé, G. Meligrana, C. Gerbaldi, *ACS Appl. Mater. Interfaces* **2019**, *2*, 3, 1600–1607.
[59] V. Chaudoy, J. Jacquemin, F. Tran-Van, M. Deschamps, F. Ghamouss, *Pure Appl. Chem.* **2019**, *91*, 8, 1361–1381.
[60] P.-E. Delannoy, B. Riou, B. Lestriez, D. Guyomard, T. Brousse, J. le Bideau, *J. Power Sources.* **2015**, *274*, 1085–1090.

Manuscript received: February 8, 2021
Revised manuscript received: April 21, 2021
Accepted manuscript online: April 21, 2021
Version of record online: June 10, 2021